www.sciencemag.org/cgi/content/full/science.aad5725/DC1

Supplementary Material for

Postnatal genome editing partially restores dystrophin expression in a mouse model of muscular dystrophy

Chengzu Long, Leonela Amoasii, Alex A. Mireault, John R. McAnally, Hui Li, Efrain Sanchez-Ortiz, Samadrita Bhattacharyya, John M. Shelton, Rhonda Bassel-Duby, Eric N. Olson*

*Corresponding author. E-mail: eric.olson@utsouthwestern.edu

Published 31 December 2016 on *Science* Express
DOI: 10.1126/science.aad5725

This PDF file includes:

Materials and Methods

Plasmids. The pSpCas9(BB)-2A-GFP (PX458) plasmid containing the human codon optimized SpCas9 gene with 2A-EGFP and the backbone of sgRNA was a gift from Feng Zhang (Addgene plasmid #48138) *(30).* Cloning of sgRNA was done according to the Feng Zhang Lab CRISPR plasmid instructions (*30*). AAV9 CRISPR/Cas9 vectors (miniCMV-Cas9-shortPolyA and pBSU6-FE-RSV-GFP plasmid) were obtained from Dr. Dirk Grimm (Heidelberg University Hospital).

Transfection of 10T½ cells with pSpCas9(BB)-2A-GFP (PX458) plasmid. Cells were transfected by Lipofectamine 2000 Transfection Reagent (ThermoFisher Scientific) according to the manufacturer's instructions and the cells were incubated for a total of 48 to 72 h.

Cell sorting of transfected 10T½ cells. Cell sorting was performed by the Flow Cytometry Core Facility at UT Southwestern Medical Center. Transfected cells were dissociated using Trypsin-EDTA solution. The mixture was incubated for 5 min at 37 °C and 2 ml of warm DMEM medium supplemented with 10%FBS was added. The re-suspended cells were transferred into a 15-ml Falcon tube and gently triturated 20 times. The cells were centrifuged at 1300 rpm for 5 min at room temperature. The medium was removed and the cells were re-suspended in 500 µl of PBS supplemented with 2% BSA. Cells were filtered into a cell strainer tube through its mesh cap. Sorted single cells were separated into microfuge tubes into GFP+ and GFP- cell populations.

Isolation of genomic DNA from sorted cells. Protease K (20mg/ml) was added to DirectPCR Lysis Reagent (Viagen Biotech Inc.) to a final concentration of 1mg/ml. Cells

were centrifuged at 4°C, at 6000 rpm for 10 min and the supernatant was discarded. Cell pellets kept on ice were resuspended in 50~100uL DirectPCR/Protease K solution and incubated at 55°C for >2 hr or until no clumps were observed. Crude lysates were incubated at 85°C for 30 min, and then spun for 10 sec. NaCl was added to a final concentration of 250 mM, followed by the addition of 0.7 volumes of isopropanol to precipitate DNA. The DNA was centrifuged at 4°C, at 13000 rpm for 5 min and the supernatant was discarded. The DNA pellet was washed with 1 ml of 70% EtOH, and dissolved in water or TE. The DNA concentration was measured using a Nanodrop instrument (Thermo Scientific).

Amplifying the target genomic region by PCR. PCR assays contained 2 µl of GoTaq (Promega), 20 µl of 5X Green GoTaq Reaction Buffer, 8 µl of 25mM $MgCl_2$, 2µl of 10µM primer (Dmd_842F and Dmd_842R) **(Table S3)**, 2µl of 10mM dNTP, 4 µl of genomic DNA, and ddH_2O to 100 µl. PCR conditions were: 94ºC for 2 min; 32X (94ºC for 15 sec, 59ºC for 30 sec, 72ºC for 1 min); 72ºC for 7 min; followed by 4ºC. PCR products were analyzed by 2% agarose gel electrophoresis and purified from the gel using the QIAquick PCR Purification Kit (Qiagen) for direct sequencing. These PCR products were subcloned into pCRII-TOPO vector (Invitrogen) according to the manufacturer's instructions. Individual clones were picked and the DNA was sequenced.

T7E1 analysis of PCR products. Mismatched duplex DNA was obtained by denaturation/renaturation of 25 µl of the genomic PCR samples using the following conditions: 95ºC for 10 min, 95ºC to 85ºC (-2.0ºC/s), 85ºC for 1 min, 85ºC to 75ºC (-0.3ºC/s), 75ºC for 1 min, 75ºC to 65ºC (-0.3ºC/s), 65ºC for 1 min, 65ºC to 55ºC (-

0.3ºC/s), 55ºC for 1 min, 55ºC to 45ºC (-0.3ºC/s), 45ºC for 1 min, 45 ºC to 35 ºC (-0.3ºC/s), 35ºC for 1 min, 35ºC to 25ºC (-0.3ºC/s), 25ºC for 1 min, hold at 4ºC.

Following denaturation/renaturation, the following was added to the samples: 3 µl of 10X NEB buffer 2, 0.3 µl of T7E1 (New England BioLabs), and ddH_2O to 30 µl. Digestion reactions were incubated for 1 hour at 37ºC. Undigested PCR samples and T7E1 digested PCR products were analyzed by 2% agarose gel electrophoresis.

Cas9 mRNA. The Cas9 mRNA (5meC, Ψ) was purchased from TriLink Biotechnologies (L-6125).

In vitro transcription of sgRNA. T7 promoter sequence was added to the sgRNA template by PCR. The gel purified PCR products were used as template for in vitro transcription using the MEGAshortscript T7 Transcription Kit (ThermoFisher Scientific). sgRNA were purified by MEGAclear Transcription Clean Up Kit (ThermoFisher Scientific) and eluted with nuclease-free water (Ambion). The concentration of guide RNA was measured by a NanoDrop instrument (Thermo Scientific).

CRISPR/Cas9-mediated genomic editing by one-cell embryo injection. All animal procedures were approved by the Institutional Animal Care and Use Committee at the University of Texas Southwestern Medical Center. C57BL/10ScSn-*Dmd*^{mdx}/J mice were used as oocyte donors. Superovulated female B6C3F1 mice (6 weeks old) were mated to B6C3F1 stud males. Superovulated female homozygote C57BL/10ScSn-*Dmd*^{mdx}/J (12-18 grams) were mated to hemizygote C57BL/10ScSn-*Dmd*^{mdx}/J stud males. Zygotes were harvested and kept in M16 medium (Brinster's medium for ovum culture with 100U/ml penicillin and 50 mg/ml streptomycin) at 37^{o}C for 1 hour. Zygotes were

transferred to M2 medium (M16 medium and 20 mM HEPES). Cas9 mRNA and sgRNAs were injected into the pronucleus and cytoplasm. Different doses of Cas9 mRNA and sgRNA were injected into zygotes, as detailed in **Table S2**. Injected zygotes were cultured in M16 medium for 1 hour at 37^{o}C and then transferred into the oviducts of pseudopregnant ICR female mice.

rAAV. rAAV9 vectors expressing Cas9, sgRNA-mdx or sgRNA-R3 were produced and purified by the Harvard Medical School/Boston Children's Hospital Viral Core. Titers are expressed as viral genomes per ml (vg/ml) and rAAV titers used for injection in mice were 2X10^{14} vg/ml.

AAV-transduction of *mdx* mice. For rAAV injections, *mdx* mice were anesthetized by intraperitoneal (IP) injection of ketamine and xylazine anesthetic cocktail. For intra muscular (IM) injection, tibialis anterior (TA) muscle of P12 male *mdx* mice was injected with 50 µl of AAV9 preparations, or saline solution. For retro-orbital (RO) injection, P18 male *mdx* mice were injected with 90 µl of AAV9 preparations, or saline solution. For IP injection, P1 *mdx* mice were injected using a syringe (29G) with 30 µl of AAV9/1 preparations, or saline solution. For a second type of IP injection, we optimized the injection in P1 *mdx* mice by using an ultrafine syringe (31G) and injected with 50 µl of AAV9 preparations, or saline solution. Animals were housed in a temperature-controlled room (19–22°C) with a 12:12-h light/dark cycle. Mice were euthanized by CO_2 inhalation followed by cervical dislocation. Skeletal muscle and heart were dissected 3- and 6-weeks after IM injection, 4-, 8- and 12-weeks after RO injection and 4 and 8 weeks after IP injection. Tissues were frozen in nitrogen-cooled isopentane and liquid nitrogen for histological and immunoblot assays, respectively.

Isolation of RNA. RNA was isolated from muscle using TRIzol RNA Isolation Reagent (ThermoFisher Scientific) according to the manufacturer's instructions.

Isolation of tail DNA for genotyping. Tail biopsies were added to 100µl of 25mM NaOH / 0.2 mM EDTA solution and placed at 95ºC for 15 min and then cooled to room temperature. Following the addition of 100µl of 40 mM Tris-HCl (pH 5.5), the tubes were centrifuged at 15,000 x g for 5 min. DNA samples were kept at 4ºC for several weeks or at –20ºC for long-term storage.

Isolation of tissue DNA for PCR. DNA was isolated from muscle tissues using DirectPCR Lysis Reagent (Viagen Biotech Inc.), according to the manufacturer's instructions.

Grip strength test. Muscle strength was assessed by a grip strength behavior task performed by the Neuro-Models Core Facility at UT Southwestern Medical Center. The 4- and 8-week-old mice were removed from the cage, weighed and lifted by the tail causing the forelimbs to grasp the pull-bar assembly connected to the grip strength meter (Columbus Instruments). The mouse was drawn along a straight line leading away from the sensor until the grip is broken and the peak amount of force in grams was recorded. This was repeated 5 to 6 times (*31*). All measurements were performed in a blinded fashion.

Serum creatine kinase (CK) measurement. Mouse serum CK was measured by the Metabolic Phenotyping Core at UT Southwestern Medical Center. Blood was collected from the submandibular vein and serum CK level was measured by VITROS Chemistry

Products CK Slides to quantitatively measure CK activity using VITROS 250 Chemistry System.

Histological analysis of muscles and morphometric analysis. Histological analysis of muscles was performed as described previously (*7*). Morphometric analyses of dystrophin-positive and total myofibers and cardiomyocytes were carried out on replicates of whole step-sections of TA muscles and hearts scanned at 20x objective magnification. Scanned images, ranging in size from 7889 x 7570 pixels to 27518 x 18466 pixels, were parsed using Nikon Imaging Solution Elements v4.20.00 Software's Annotations and Measurements functions (NIS/AM). Dystrophin positive myofibers and cardiomyocytes were individually counted and recorded using NIS/AM. The total number of myofibers and cardiomyocytes in a section were estimated from the cell-counts of eight 20x objective sub-section field areas and extrapolated to the area of the whole section.

Western blot analysis. Western blot was performed as described previously (*7*) Antibodies to dystrophin (1:1000, D8168, Sigma-Aldrich), vinculin (1:1000, V9131, Sigma-Aldrich), GAPDH (1:8000, MAB374, Millipore), goat anti-mouse and goat-anti rabbit HRP-conjugated secondary antibodies (1:3000, Bio-Rad) were used for described experiments.

Off-target sites analysis. Target and potential off-target loci **(Table S4)** were amplified by PCR using primers listed in **Table S3** for (-) *mdx* and (+) *mdx*+Cas9 (four mice for each group). PCR products were subject to T7E1 assay as described.

Statistics. Values are given as mean standard error or standard deviation. Differences between respective two groups (*mdx* and *mdx*-AAV, *mdx*-AAV and WT) were assessed using unpaired two-tailed Student's t-tests. $P<0.05$ was regarded as significant. Statistical analysis was performed in Excel (Microsoft). Additionally, differences between all three groups were assessed using Anova statistical analysis in Prism6 (GraphPad software).

Semi-quantitative immunohistochemistry and densitometric analysis. Semi-quantitative immunohistochemistry was performed to quantify and relate dystrophin expression levels (*32*-*33*) among WT, *mdx*, and IP-AAV-8wks, IM-AAV-6wks, and RO-AAV-8wks (TA) or RO-AAV-12wks (heart) treated *mdx* mice. Using Arechavala-Gomeza *et al* as a framework, 8-bit images of dystrophin and laminin co-stained immunofluorescence were acquired from three non-overlapping, 20x objective field areas of tibialis anterior muscle and ventricular myocardium, from each of three mice per group. Images were acquired on a Leica DM2000 epifluorescence photomicroscope equipped with an Optronics MicroFire Bayer-masked Color CCD camera. Optronics Picture Frame 2.0 acquisition software was used to set exposure independently for dystrophin (rhodamine) and laminin (fluorescein), and acquire 1600x1200 pixel greyscale images. Exposure was set just below saturation for each fluorophore channel. Analysis of resulting images was conducted using ImageJ 1.48 software (NIH, Bethesda, MD) on centroid 700x700 pixel crops, where 10 40-pixel circular regions-of-interest areas (ROIs) were spatially adjusted to each of their nearest sarcolemmal boundaries. Measures for mean-pixel-intensity, standard-deviation-pixel-intensity, modal-pixel-intensity, minimum-pixel-intensity, maximum-pixel-intensity, and integrated-density were

made and saved for each 40-pixel circular ROI and alternate fluorophore channel (90 dystrophin per animal group, 90 same-field laminin per group). Numerical indices were exported from ImageJ to Microsoft Excel. Mathematical and statistical operations in Excel were used to calculate sarcolemmal dystrophin stain integrated densities, normalized to sarcolemmal laminin stain integrated densities. For both stains, cytoplasmic minimum pixel intensity for each fluorophore and independent ROI were subtracted from the integrated density. Mean integrated density ± standard deviation for tibialis anterior was calculated for each animal group and charted as a histogram. A separate histogram was charted for ventricular myocardium.

Supplementary Materials References

30. F. A. Ran *et al.*, *Nat Protoc* **8**, 2281-2308 (2013).

31. R. Willmann *et al.*, *Neuromuscul Disord* **22**, 43-49 (2012).

32. V. Arechavala-Gomeza *et al.*, *Neuropathol Appl Neurobiol* **36**, 265-274 (2010).

33. K. Anthony *et al.*, *Neurology* **83**, 2062-2069 (2014).

Supplementary Figures

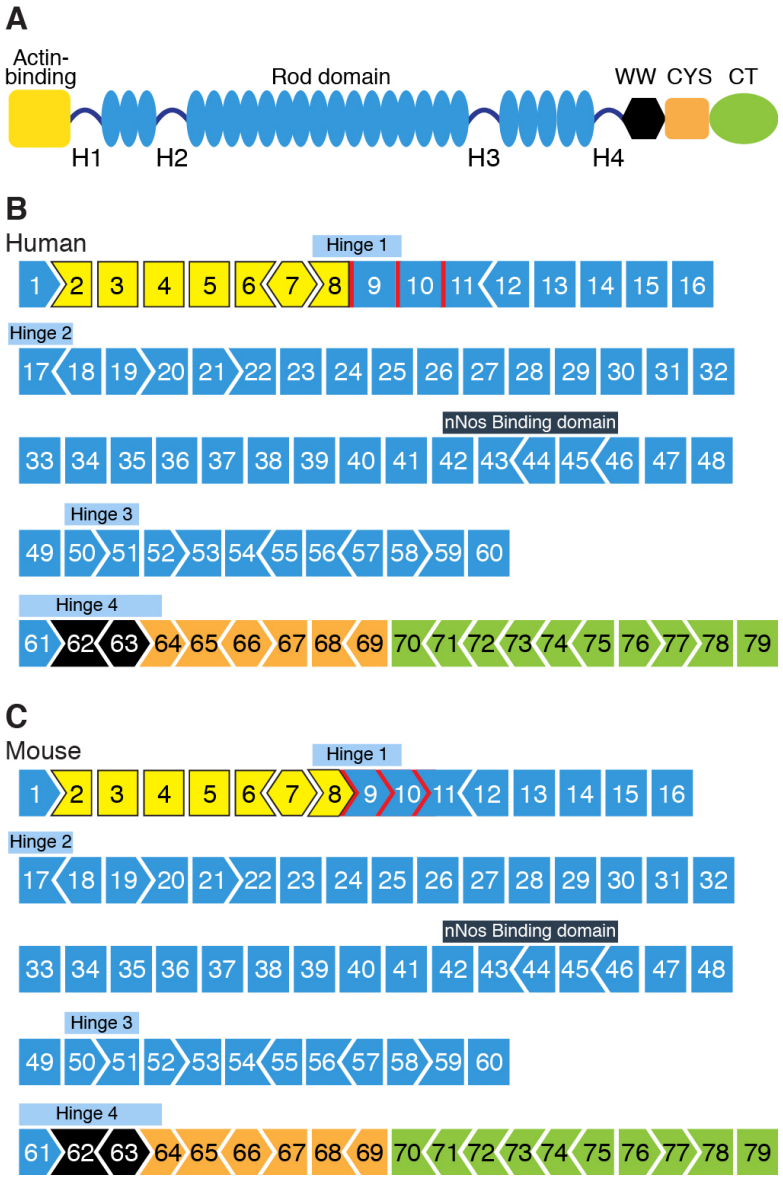

Fig. S1. Major protein functional domains and exon structure of dystrophin gene. **(A)** Domains of dystrophin protein are color-coded on the corresponding exons. **(B and C)** Human and mouse dystrophin gene exon structure. Shapes of intron-exon junctions indicate complementarity that maintains the open reading frame upon splicing. Red lines indicate the three different intron-exon junctions between the human and mouse genes.

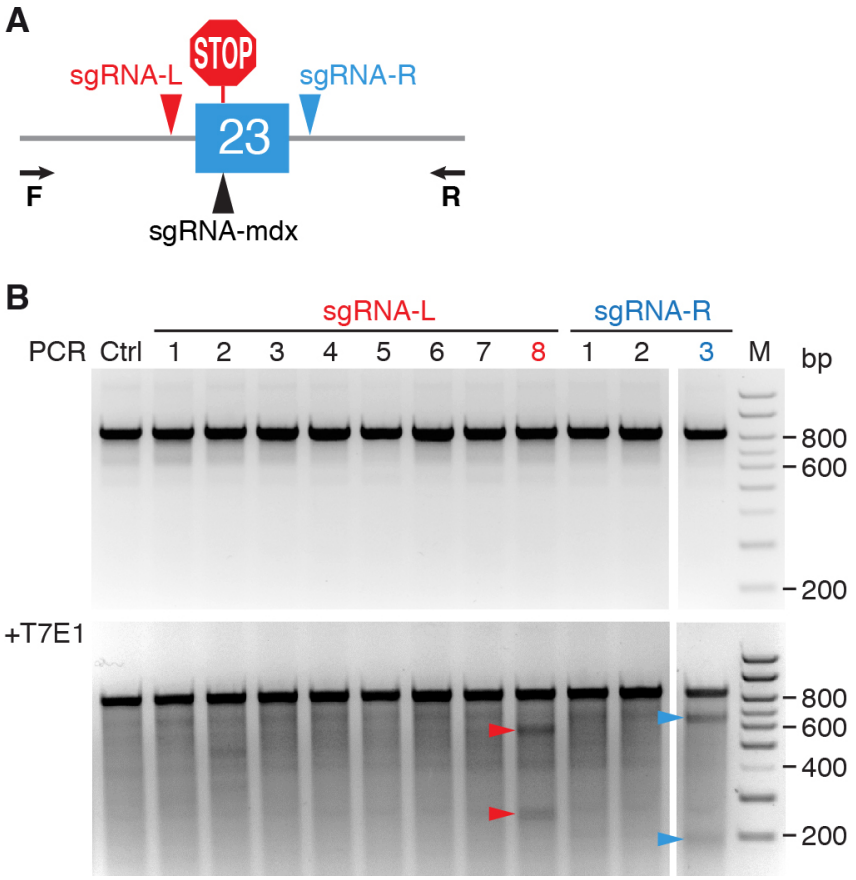

Fig. S2. Screen of guide RNAs in 10T½ cells for exon-skipping of exon 23. (A) Guide RNAs, sgRNA-L and sgRNA-R, which target the 5' and 3' ends of exon 23, are indicated by red and blue arrowheads, respectively. Guide RNA sgRNA-mdx which targets the premature stop codon, is indicated by a black arrowhead. **Table S1** shows sequence of sgRNAs. **(B)** Undigested PCR products (upper panel) and T7E1 digestion (lower panel) on a 2% agarose gel. Red and blue arrowheads in the lower panel indicate the cut bands by T7E1 assay from guide RNA sgRNA-L8 and sgRNA-R3, respectively. M denotes size marker lane. bp indicates the length of the marker bands.

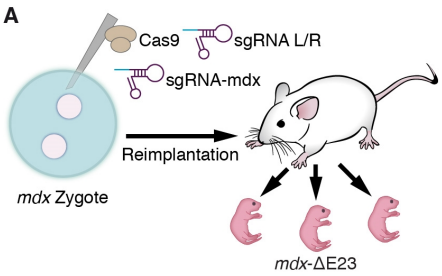

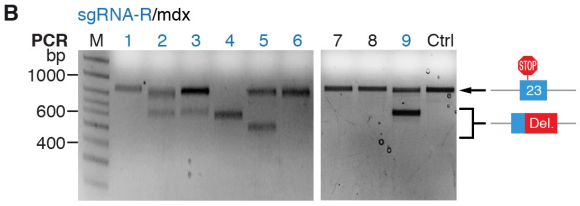

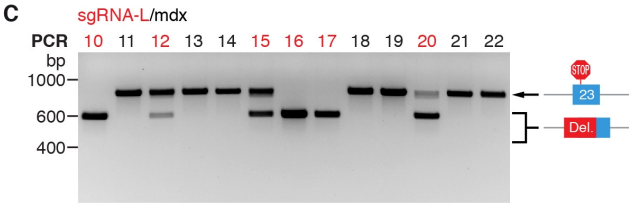

D

#	Sequence	Del.(bp)
mdx:	aacttctatttaattttgagGCTCTGCAAA//AAAATTTCAGgtaagccgaggtttggcctt	
02:	aa----------//--AATTTCAGgtaagccgaggtttggcctt	-223
03:	aacttctatttaattttgagGCTCTGCAAA----------gtttggcctt	-213
04:	aacttctatttaattttgagGCTCTGCAAA//----------	-230
05:	----------//AAAATTTCAGgtaagccgaggtttggcctt	-315
06:	aacttctatttaattttgagGCTCTGCAAA//----------tt	-41
09:	aacttctatttaattttgagGCTCTGCAAA----------	-252

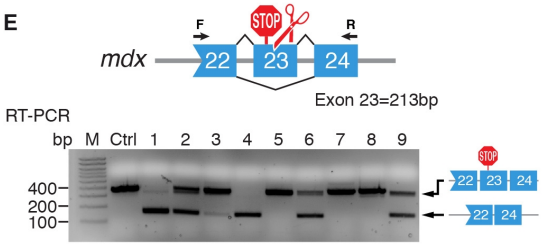

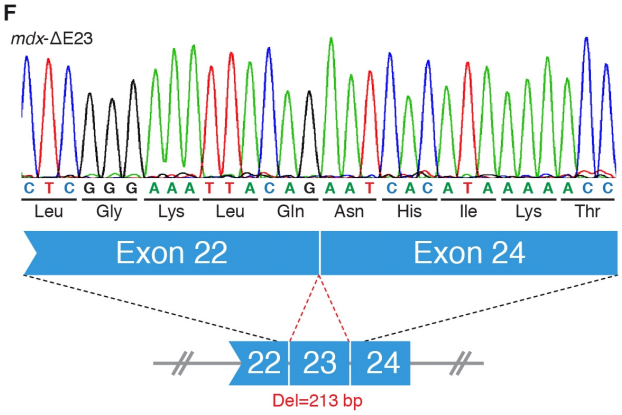

Fig. S3. Myoediting-mediated exon-skipping in the germline of *mdx* mice. (A) Strategy for exon-skipping in the germline of *mdx* mice. Cas9 mRNA and sgRNAs were co-injected into *mdx* eggs, which were reimplanted into pseudopregnant foster mothers, and offspring were analyzed for exon skipping. **(B and C)** Primers (F and R) shown in **fig. S2A** and **Table S1** were used to generate PCR products corresponding to *Dmd* exon 23 from pups, which were analyzed on an agarose gel. Panel B shows PCR products obtained in offspring edited with sg-RNA-R3 and sgRNA-mdx, and panel C shows PCR products obtained in offspring edited with sgRNA-L8 and sgRNA-mdx. The upper band indicates the full-length PCR products and the lower bands indicate PCR products with deletions encompassing exon 23. Seven out of 9 pups in panel B and 5 out of 13 pups in panel C contain evident deletions that skip exon 23. M denotes size markers. Blue and red numbers indicate positive *mdx* pups with large or small indel mutations. **(D)** Sequencing results of PCR products from mouse #02 to 06 showing NHEJ-mediated deletion of exon 23. **(E)** RT-PCR of muscle RNA from WT and germline edited *mdx* mice was performed with the indicated sets of primers (F and R) (**Table S3**). Deletion of exon 23 allows splicing from exon 22 to 24 (lower band) and restoration of the *Dmd* open reading frame. M denotes size marker lane. bp indicates the length of the marker bands. **(F)** Sequencing results of RT-PCR product from mdx-ΔE23 mouse showing rescue of the open reading frame.

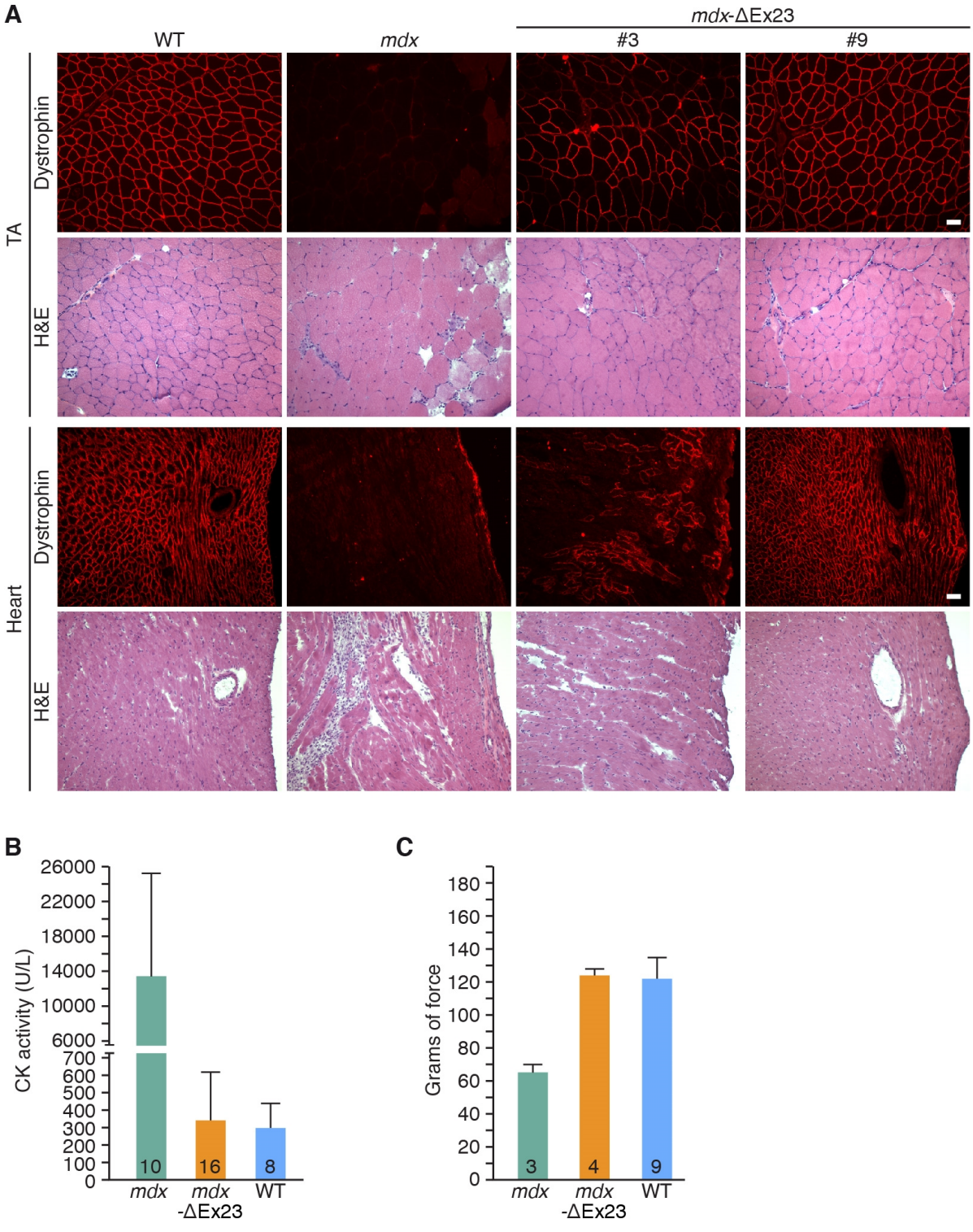
A
WT
mdx
mdx-ΔEx23
#3
#9
TA
Dystrophin
H&E
Heart
Dystrophin
H&E
B
CK activity (U/L)
26000
22000
18000
14000
10000
6000
700
600
500
400
300
200
100
0
10
16
8
mdx
mdx -ΔEx23
WT
C
Grams of force
180
160
140
120
100
80
60
40
20
0
3
4
9
mdx
mdx -ΔEx23
WT

Fig. S4. Histological and functional analysis of muscle from germline edited *mdx* mice by skipping exon 23. (A) Dystrophin immunostaining (red) and H&E staining of muscle (TA and heart) from *mdx* mice and *mdx* mice following NHEJ mediated skipping of exon 23 (*mdx*-ΔEx23) is shown. Dystrophin expression is restored by skipping exon 23. Histological sections from two different mice (#3 and #9, **Fig. S3B**) with low and high percentage of Myoediting, respectively, are shown. **(B)** Serum creatine kinase (CK), a diagnostic marker for muscular dystrophy that reflects muscle leakage, was measured in *mdx*, *mdx*-ΔEx23 and WT mice. Consistent with the histological results, serum CK levels of the *mdx*-ΔEx23 mice were substantially decreased compared to *mdx* mice. **(C)** *mdx*, *mdx*-ΔEx23 and WT mice were subjected to grip strength testing to measure muscle performance, and the *mdx*-ΔEx23 mice showed enhanced muscle performance compared to *mdx* mice at 8 weeks of age. The number of mice for each group is labeled on the bar. Data are presented as mean ± SD.

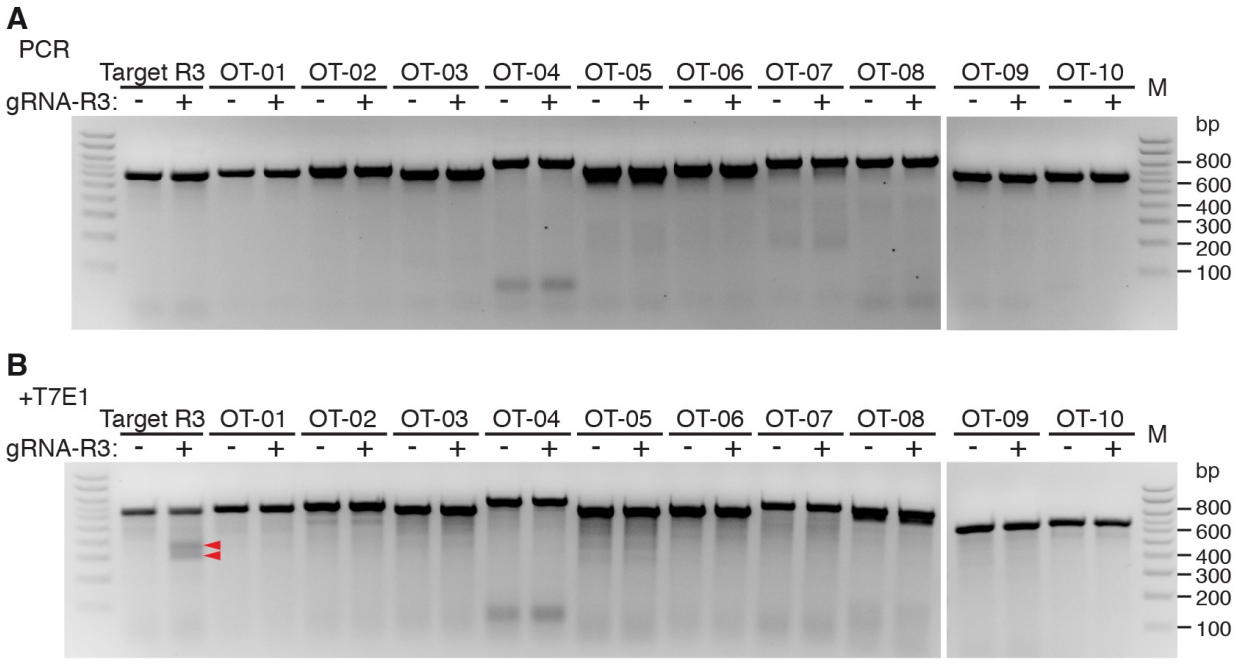

Fig. S5. Off-target analysis of guide RNA-R3. (A) Undigested PCR products and **(B)** T7E1 digestion from T7E1 assay on *Dmd* (Target) site and genome-wide "top ten" theoretical off-target sites (OT-01 to OT-10) (**Table S4**). The red arrowheads indicate cut bands by T7E1. – and + denote the genomic DNA from control *mdx* groups and Myoedited *mdx* groups (four mice for each group).

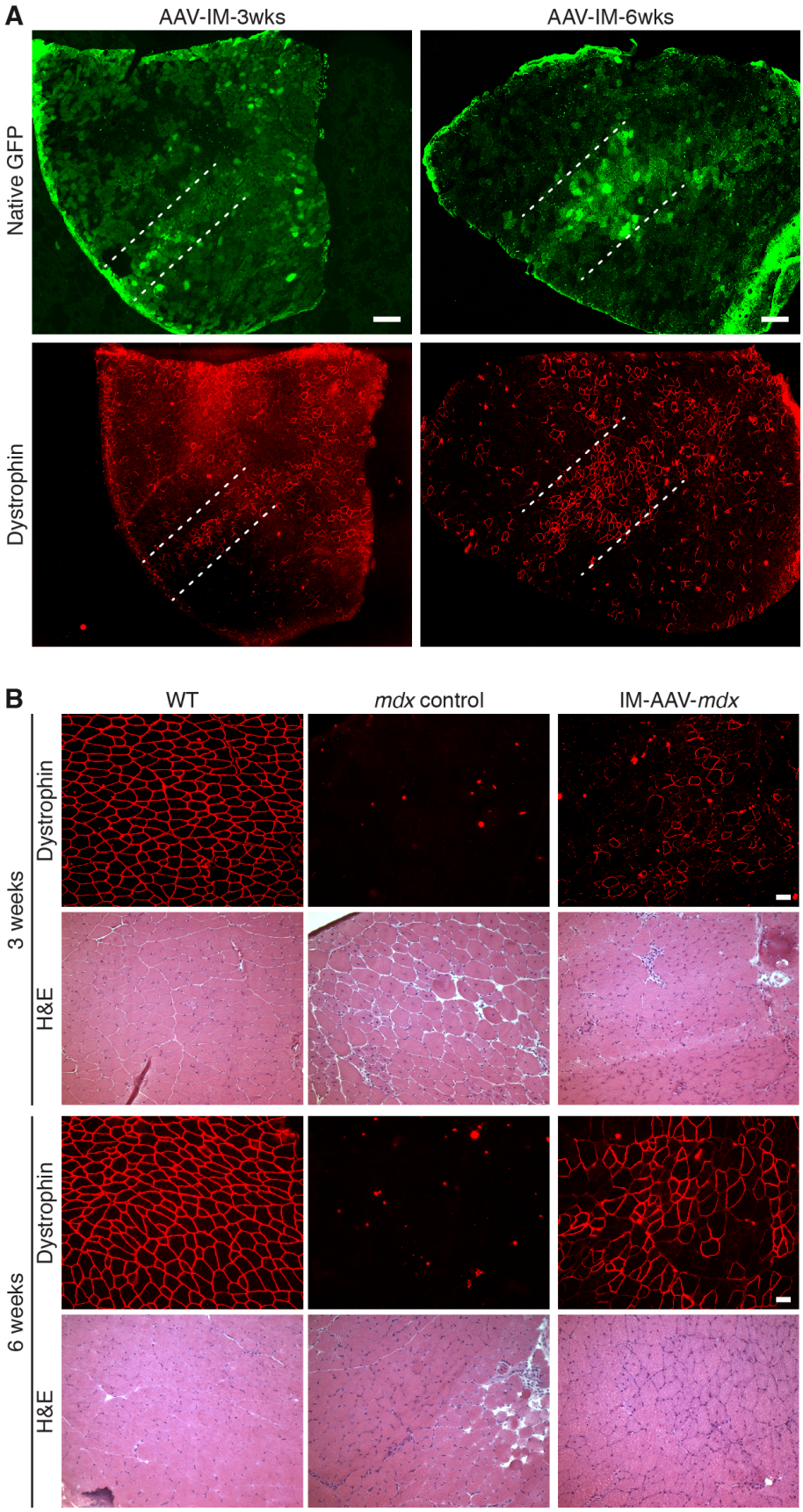
A
AAV-IM-3wks
AAV-IM-6wks
Native GFP
Dystrophin
B
WT
mdx control
IM-AAV-mdx
3 weeks
6 weeks
Dystrophin
H&E

Fig. S6. Rescue of dystrophin expression in postnatal *mdx* mice by direct intramuscular injection of AAV9. (A) Native green fluorescent protein (GFP) and dystrophin immunostaining from serial sections of *mdx* mouse TA muscle is shown 3- and 6-weeks post-IM of AAV9-Cas9 and AAV9-gsRNA-GFP (IM-AAV at P12). Dotted lines indicate the injection needle track. Scale bar, 200 microns**. (B)** Progressive rescue of dystrophin expression in *mdx* mice by Myoediting with IM-AAV. Dystrophin immunostaining and H&E staining of TA muscle is shown for WT, *mdx* and IM-AAV treated *mdx* mice at 3- and 6-weeks post-injection. Transduction frequency (rescue) increased to an estimated 25.5±2.9% (SD) of myofibers by 6-week post-IM-AAV (three male *mdx* mice for each group). Scale bar, 40 microns**.**

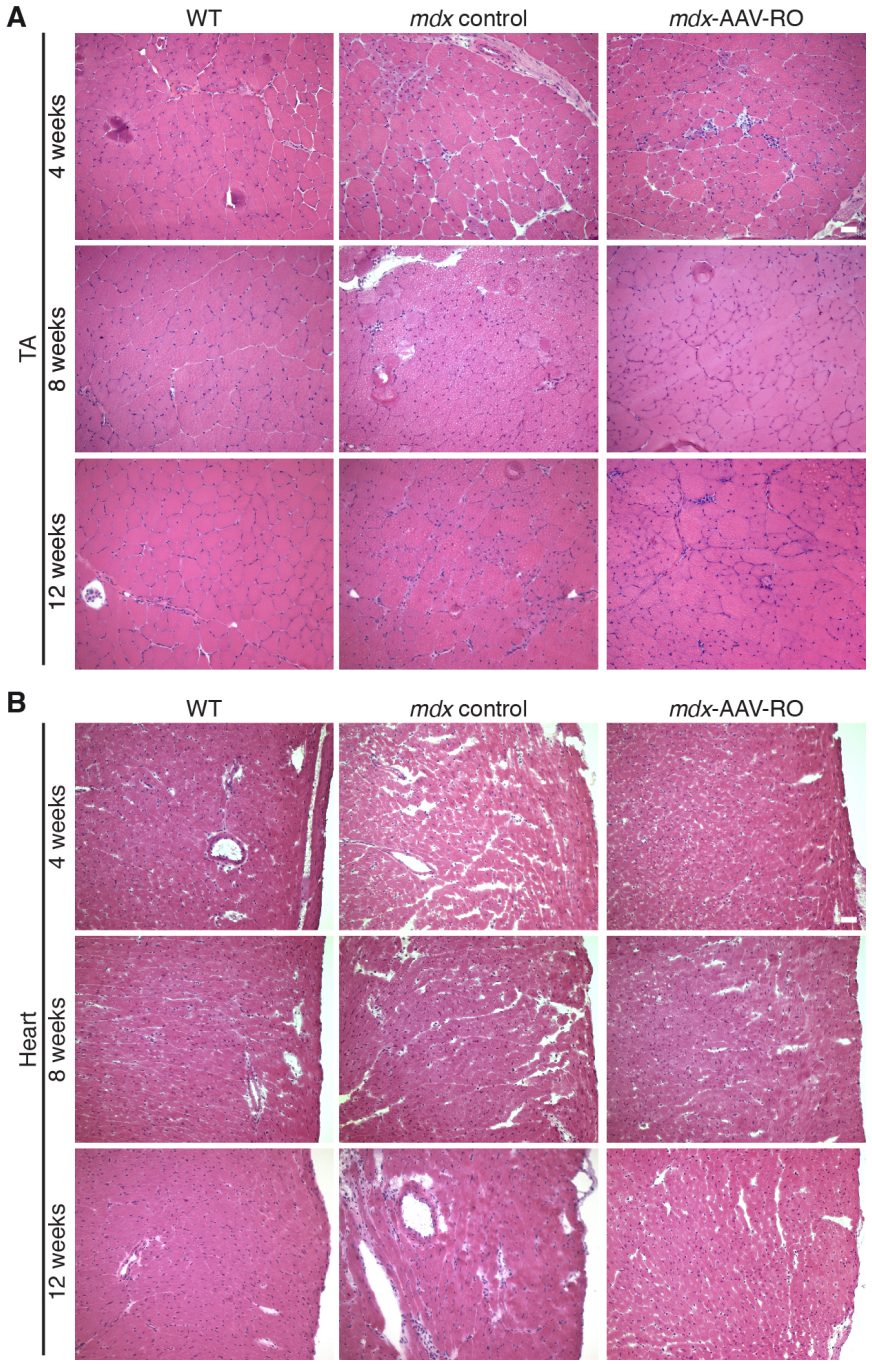

Fig. S7. Progressive rescue of dystrophin expression in postnatal *mdx* mice by retro-orbital injections of Myoediting components. H&E staining of TA and heart from WT, *mdx* and edited *mdx* at 4-, 8- and 12-weeks post-RO-AAV injection. Scale bar, 40 microns.

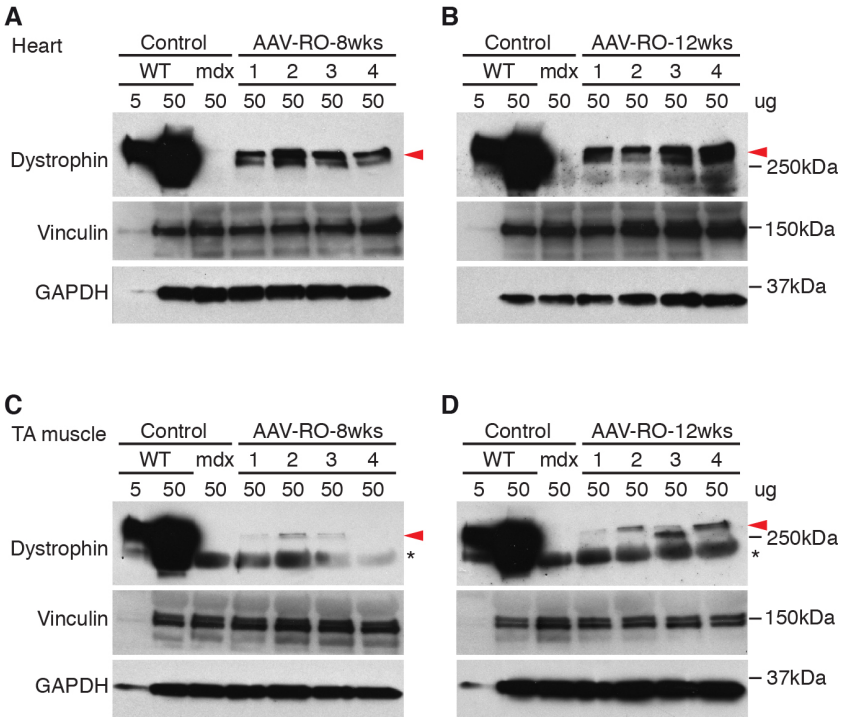

Fig. S8. Western blot analysis of dystrophin expression in muscle from postnatal *mdx* mice with retro-orbital injection of Myoediting components. Western blot analysis of (**A and B**) heart and (**C and D**) TA (5 or 50 ug of protein) from WT, *mdx*, and *mdx*-AAV-RO mice at 8- and 12-weeks post-RO-injection. Red arrowhead (above 250kD) indicates the immunoreactive bands of dystrophin. Four male *mdx* mice for each group. Asterisk indicates non-specific immunoreactive bands in TA. GAPDH and vinculin are loading controls. kDa indicates protein molecular weight.

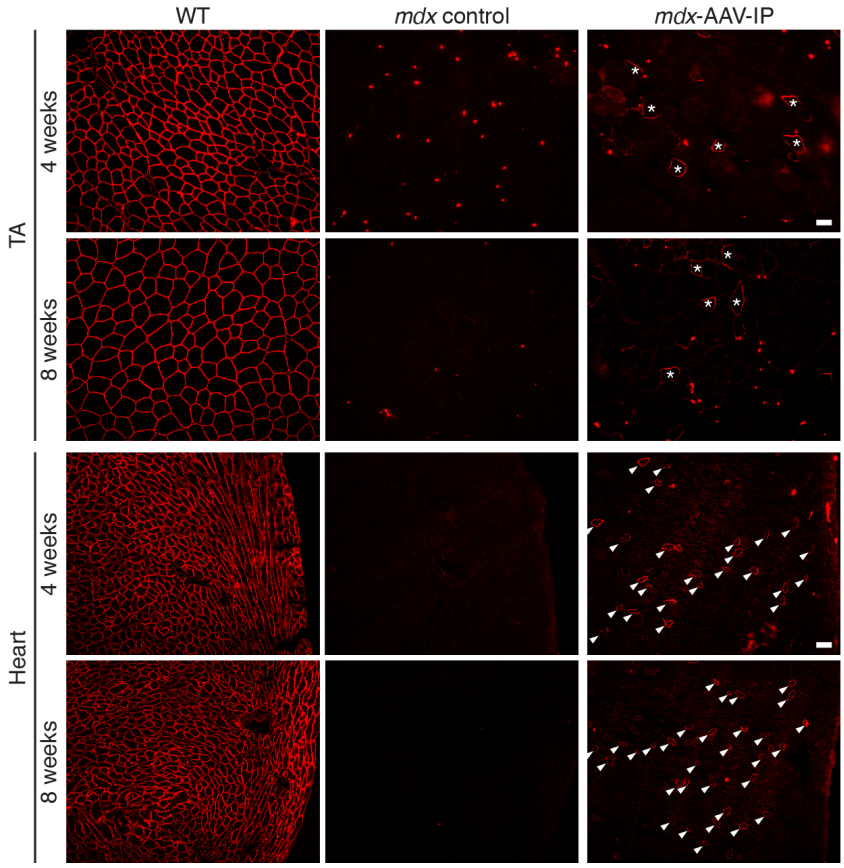

Fig. S9. Rescue of dystrophin expression in postnatal *mdx* mice by intraperitoneal injection (IP) of Myoediting components. Dystrophin immunostaining (red) of TA and heart is shown for WT, *mdx*, and IP-AAV treated *mdx* (*mdx*-AAV-IP) mice at 4- and 8-weeks post-IP injection at P1. A transduction frequency (rescue) of 1.4±1.1% (SD) of myofibers is calculated in Myoedited *mdx* mouse TA muscle (three mice for each group), and 1.1±1.1% (SD) of cardiomyocytes in edited *mdx* mouse heart (three mice for each group), at 4-weeks post-IP-AAV. At 8-weeks post-IP-AAV, 1.8±1.2% (SD) of myofibers in TA and 3.2±2.4% (SD) of cardiomyocytes show dystrophin expression. Asterisks and arrowheads indicate dystrophin positive myofibers and cardiomyocytes, respectively, in IP-AAV edited *mdx* mice. Scale bar, 40 microns.

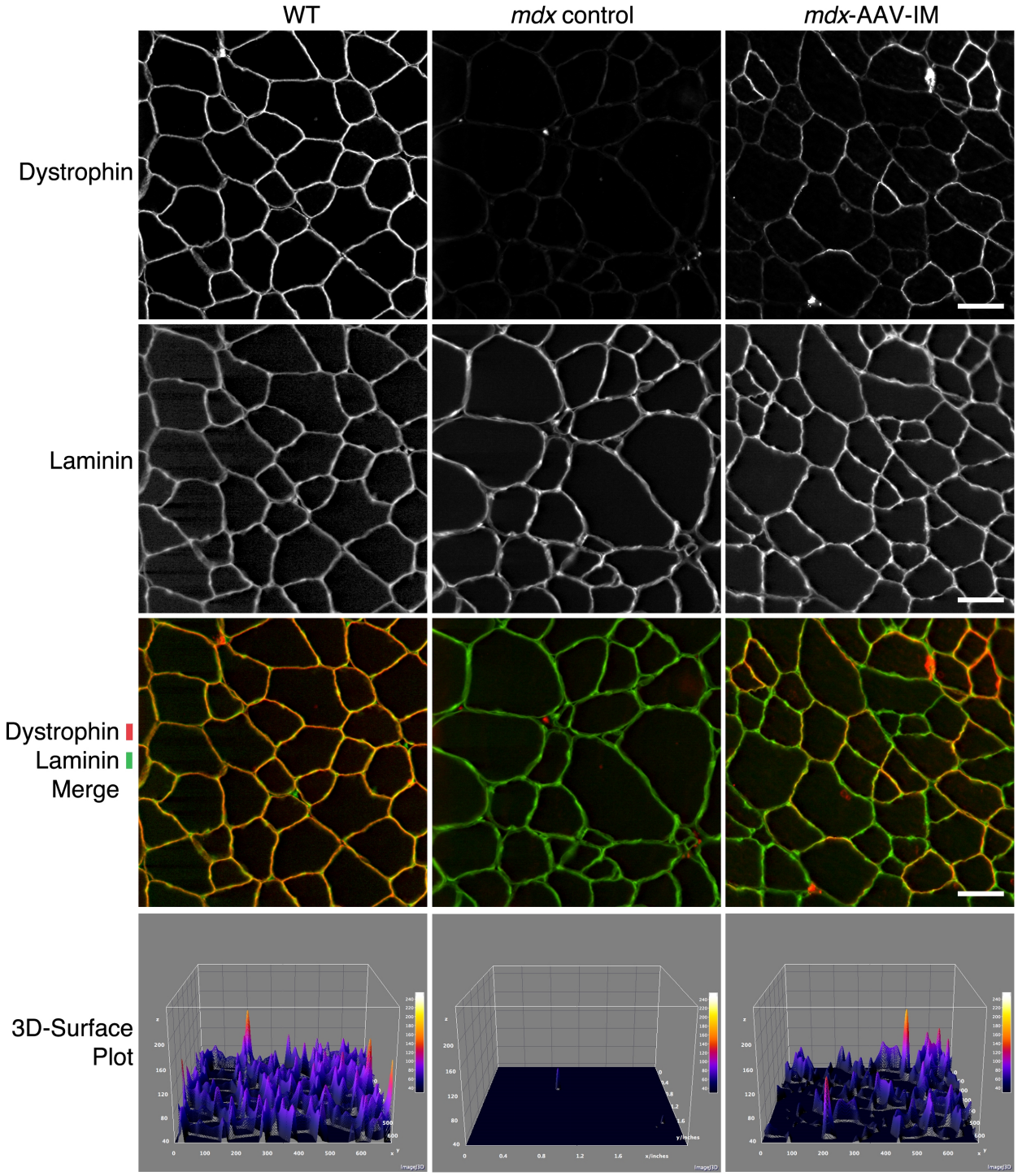

Fig. S10. Comparative analysis of sarcolemma-associated dystrophin and laminin protein abundance in skeletal muscle by immunohistochemistry. Relative abundance of dystrophin and laminin proteins is shown by immunostaining of tibialis

anterior (TA) muscle from WT, *mdx*, and IM-AAV edited *mdx* mice. Greyscale (upper panels) and merged-pseudocolored overlays (dystrophin (red) and laminin (green) in middle panels) show baseline protein levels of dystrophin and laminin in WT, absence of dystrophin in *mdx*, and restored dystrophin in IM-AAV edited *mdx* muscle. 3D surface plots of dystrophin staining intensity (lower panels), graphically illustrate the relative abundance of dystrophin in TA muscle across the three groups.

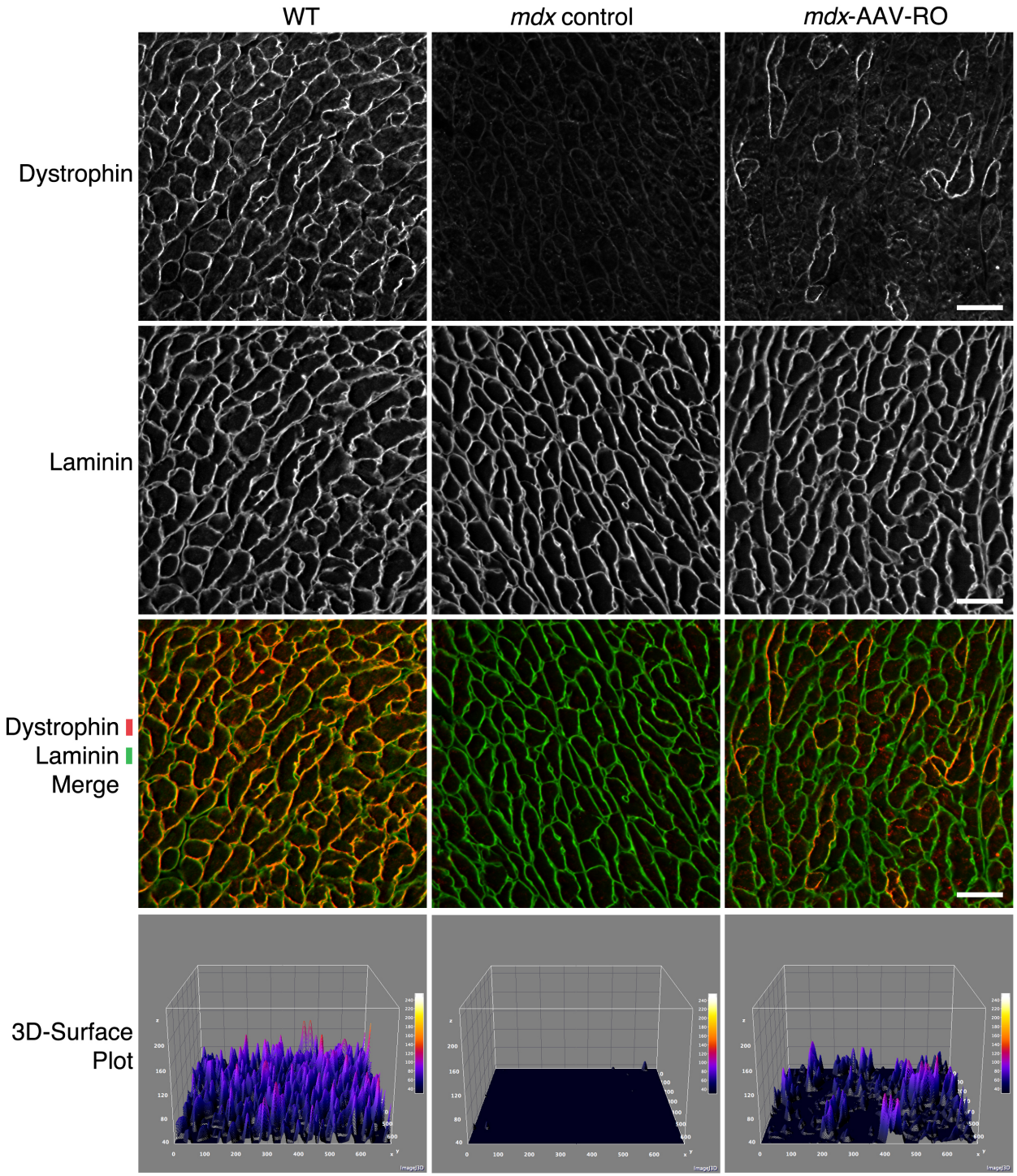

Fig. S11. Comparative analysis of sarcolemma-associated dystrophin and laminin protein abundance in cardiac muscle by immunohistochemistry. Relative abundance of dystrophin and laminin proteins is shown by immunostaining of ventricular

myocardium from WT, *mdx*, and RO-AAV edited *mdx* mice. Greyscale (upper panels) and merged-pseudocolored overlays (dystrophin (red) and laminin (green) in middle panels) show baseline protein levels of dystrophin and laminin in wild-type heart, absence of dystrophin in *mdx* heart, and restored dystrophin in RO-AAV edited *mdx* heart. 3D surface plots of dystrophin staining intensity (lower panels), graphically illustrate the relative abundance of dystrophin in ventricular myocardium across the three groups.

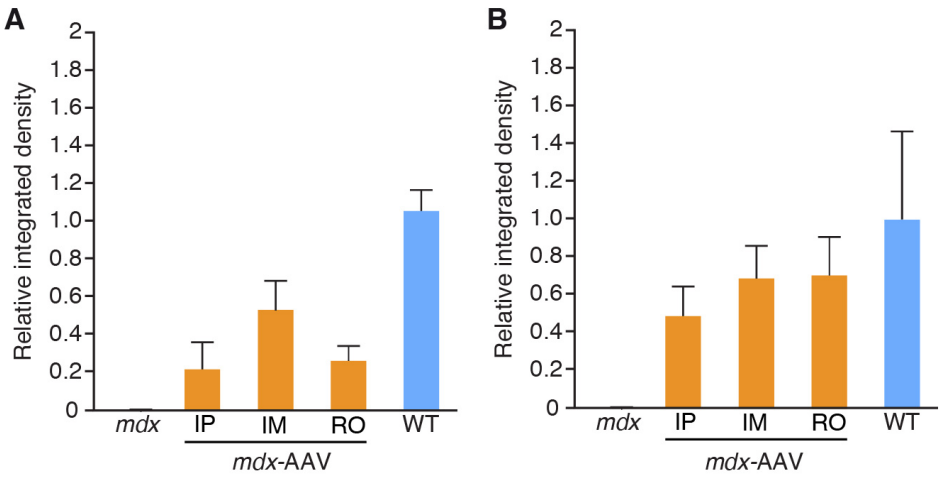

Fig. S12. Relative measure of restored dystrophin and mode of AAV delivery in skeletal and cardiac muscle by semi-quantitative immunohistochemistry. Relative integrated densities of dystrophin immunostaining in (**A**) tibialis anterior and (**B**) heart from WT, *mdx* (control), or *mdx* administered AAV Myoediting components by IP, IM, or RO at 8-, 6-, or 8-weeks post-injection, respectively. Dystrophin abundance by integrated density was measured to be percentage of WT. Data are presented as mean ± SD.

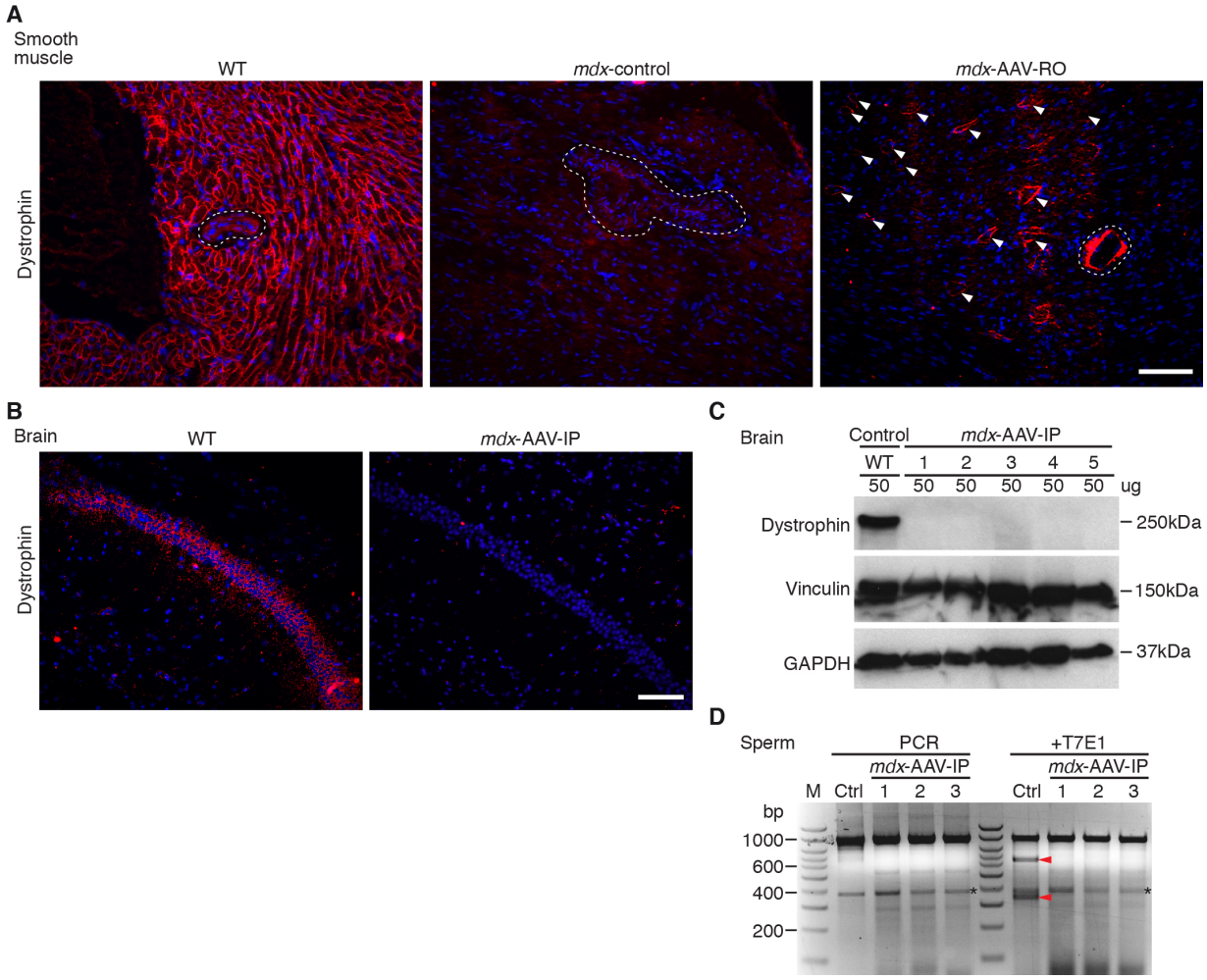

Fig. S13. Analysis of AAV-mediated gene editing in smooth muscle, brain and sperm of postnatal *mdx* mice. (A) Dystrophin immunostaining (red) of smooth muscle cells of the vasculature in heart from WT, *mdx* (control), and *mdx* mice injected RO with AAV Myoediting components. Nuclei are labeled by Hoechst dye (blue). Arrowheads indicate dystrophin positive cardiomyocytes. Dotted lines indicate the outline of vascular smooth muscle. Scale bar, 60 microns. **(B)** Dystrophin immunostaining (red) shows expression in hippocampal CA1/CA2 regions of WT and *mdx*-AAV-IP mouse brain. Scale bar, 60 microns. **(C)** Western blot analysis of brain samples from WT and *mdx*-AAV-IP mice 4- weeks post-injection. GAPDH and vinculin are loading controls. kDa

indicates protein molecular weight. **(D)** T7E1 assay on target site (*Dmd*) in sperm genomic DNA from AAV-IP injected *mdx* mice. Undigested PCR products and T7E1 digestion samples are compared. The red arrowheads indicate cut bands by T7E1 from the positive control. Asterisk indicates the non-specific PCR bands. M denotes size marker lane. bp indicates the DNA length of the marker bands.

Supplementary Tables

Table S1. Sequence of sgRNAs target *Dmd* Exon23

sgRNA#	Target site	PAM
mdx	**TCTTTGAAAGAGCAATAAAA**	**TGG**
L1	TGAACTTCTATTTAATTTTG	AGG
L2	TTTCATTCATATCAAGAAGA	AGG
L3	TGCAGAGCCTCAAAATTAAA	TAG
L4	AACTCATCAAATATGCGTGT	TAG
L5	CTCTTTCAAAGAACTTTGCA	GAG
L6	TGCTCTTTCAAAGAACTTTG	CAG
L7	TTTAATTTTGAGGCTCTGCA	AAG
L8	**ATAATTTCTATTATATTACA**	**GGG**
R1	AAACTTCGAAAATTTCAGGT	AAG
R2	CGAAAATTTCAGGTAAGCCG	AGG
R3	**ATTTCAGGTAAGCCGAGGTT**	**TGG**

Table S2. Efficiency of CRISPR/Cas9-mediated genomic editing by NHEJ

sgRNA	Cas9/sgRNAs (ng/μl)	No. of Transferred Zygotes	No. of Pups	No. of ΔEx23
mdx/R3	100/50/50	36	9	7
mdx/L8	100/50/50	68	18	9

Table S3. Oligonucleotides and primer sequences.

guide RNA sequence	
sgRNA-F+E	NNNNNNNNNNNNNNNNNNGTTTAAGAGCTATGCTGGAAACAGCATAGCAA GTTTAAATAAGGCTAGTCCGTTATCAACTTGAAAAAGTGGCACCGAGTCG GTGCTTTTTTT
Primers for genotyping	
Dmd_842F	GAGAAACTTCTGTGATGTGAGGACATA
Dmd_842R	GATATTTCTGGCATATTTCTGAAGGTG
Primers for RT-PCR	
Dmd_Ex22_F	GATCCAGCAGTCAGAAAGCAAACTC
Dmd_Ex24_R	TCAGGAAAACATCAACTTCAGCCA
Primers for OT analysis	
R3OT-01-F	TCCGGAGTTGTAATTTAGTCTGTTC
R3OT-01-R	TTGGCCCCATTAAATAGTAAAGAAT
R3OT-02-F	GACTGTACCCCAGTCTGTGAGTC
R3OT-02-R	TAAAATAATCTCACCAGAACCCAAG
R3OT-03-F	TAACATGAAAGGCCAAATATAAACC
R3OT-03-R	CATTCTTCCAGTTTCTGAACAACTT
R3OT-04-F	CTTGCTAGAAGATCTGTGTTTCTCC

R3OT-04-R	TACTAGTTGAGGGACAGTTGGTCTC
R3OT-05-F	ATAGCACTTGGAGGCTTTTAAGAAT
R3OT-05-R	CATCTCTTCCCAGGGTTATAGAAAT
R3OT-06-F	GTATTCCCAAGAGCCAGTCTGTAAT
R3OT-06-R	TACATCCTCTATCAAAGGAAACTGC
R3OT-07-F	TGAAAAGCCAGAAATCAGGTATAAA
R3OT-07-R	TCACAAACCATTGAAAAATAGACCT
R3OT-08-F	AAACCCACAACTAGAGATGAAAATG
R3OT-08-R	ATTTTCCCTTAGCTTTGCTTAATGT
R3OT-09-F	CAGCGGATTTCTACGATCTACTTTA
R3OT-09-R	AGAGACCAGGATGGGATATTAAGTT
R3OT-10-F	GCTCTTTGTGACTTATTAGGGTGAA
R3OT-10-R	TTCTACCTTCGTATTAACTGCAACC

Table S4. Sequences of the target site (*Dmd* exon23 R3) and 10 potential off-target (OT) sites in the mouse genome.

#	Sequence+PAM	score	mismatches	locus
Target R3	ATTTCAGGTAAGCCGAGGTTTGG	86		
R3OT-01	CTTTAAGGAAAGCCGAGGTTAAG	1.6	3MMs [1:5:9]	chr19:-28241363
R3OT-02	ATTTTAGTGAAGCCGAGGTTCAG	1.5	3MMs [5:8:9]	chr4:-140021837
R3OT-03	CTTTCAGGCAAGCCGAGGTACAG	0.9	3MMs [1:9:20]	chr8:-41464387
R3OT-04	ATCTCAGGAAGGCCGAGGTTGGG	0.9	3MMs [3:9:11]	chr14:-64994188
R3OT-05	TTTAAAGGTAAGCCGAGGATGGG	0.5	4MMs [1:4:5:19]	chr15:+25400284
R3OT-06	CTTGCAGCTAAGCCCAGGTTTGG	0.4	4MMs [1:4:8:15]	chr14:-120694842
R3OT-07	AGGTAAGGTAAGCCAAGGTTCAG	0.4	4MMs [2:3:5:15]	chr11:-106726353
R3OT-08	ATTACTGCTAAGCCGATGTTCAG	0.4	4MMs [4:6:8:17]	chr1:+41618873
R3OT-09	ATCTCTGGTTAGCCGAAGTTTAG	0.3	4MMs [3:6:10:17]	chr5:-106752473
R3OT-10	ATTTAAGGAAAGCCGGGGTTGGG	0.3	3MMs [5:9:16]	chr19:+37670104

References and Notes

1. K. P. Campbell, S. D. Kahl, Association of dystrophin and an integral membrane glycoprotein. *Nature* **338**, 259–262 (1989). Medline doi:10.1038/338259a0

2. J. M. Ervasti, K. Ohlendieck, S. D. Kahl, M. G. Gaver, K. P. Campbell, Deficiency of a glycoprotein component of the dystrophin complex in dystrophic muscle. *Nature* **345**, 315–319 (1990). Medline doi:10.1038/345315a0

3. R. J. Fairclough, M. J. Wood, K. E. Davies, Therapy for Duchenne muscular dystrophy: Renewed optimism from genetic approaches. *Nat. Rev. Genet.* **14**, 373–378 (2013). Medline doi:10.1038/nrg3460

4. M. Jinek, K. Chylinski, I. Fonfara, M. Hauer, J. A. Doudna, E. Charpentier, A programmable dual-RNA-guided DNA endonuclease in adaptive bacterial immunity. *Science* **337**, 816–821 (2012). Medline doi:10.1126/science.1225829

5. J. A. Doudna, E. Charpentier, The new frontier of genome engineering with CRISPR-Cas9. *Science* **346**, 1258096 (2014). Medline doi:10.1126/science.1258096

6. P. Mali, K. M. Esvelt, G. M. Church, Cas9 as a versatile tool for engineering biology. *Nat. Methods* **10**, 957–963 (2013). Medline doi:10.1038/nmeth.2649

7. C. Long, J. R. McAnally, J. M. Shelton, A. A. Mireault, R. Bassel-Duby, E. N. Olson, Prevention of muscular dystrophy in mice by CRISPR/Cas9-mediated editing of germline DNA. *Science* **345**, 1184–1188 (2014). Medline doi:10.1126/science.1254445

8. K. S. Bosley, M. Botchan, A. L. Bredenoord, D. Carroll, R. A. Charo, E. Charpentier, R. Cohen, J. Corn, J. Doudna, G. Feng, H. T. Greely, R. Isasi, W. Ji, J. S. Kim, B. Knoppers, E. Lanphier, J. Li, R. Lovell-Badge, G. S. Martin, J. Moreno, L. Naldini, M. Pera, A. C. Perry, J. C. Venter, F. Zhang, Q. Zhou, CRISPR germline engineering—the community speaks. *Nat. Biotechnol.* **33**, 478–486 (2015). Medline doi:10.1038/nbt.3227

9. P. D. Hsu, E. S. Lander, F. Zhang, Development and applications of CRISPR-Cas9 for genome engineering. *Cell* **157**, 1262–1278 (2014). Medline doi:10.1016/j.cell.2014.05.010

10. S. Zacchigna, L. Zentilin, M. Giacca, Adeno-associated virus vectors as therapeutic and investigational tools in the cardiovascular system. *Circ. Res.* **114**, 1827–1846 (2014). Medline doi:10.1161/CIRCRESAHA.114.302331

11. C. Zincarelli, S. Soltys, G. Rengo, J. E. Rabinowitz, Analysis of AAV serotypes 1-9 mediated gene expression and tropism in mice after systemic injection. *Mol. Ther.* **16**, 1073–1080 (2008). Medline doi:10.1038/mt.2008.76

12. K. E. Davies, K. J. Nowak, Molecular mechanisms of muscular dystrophies: Old and new players. *Nat. Rev. Mol. Cell Biol.* **7**, 762–773 (2006). Medline doi:10.1038/nrm2024

13. T. Yokota, W. Duddy, T. Partridge, Optimizing exon skipping therapies for DMD. *Acta Myol.* **26**, 179–184 (2007). Medline

14. H. L. Li, N. Fujimoto, N. Sasakawa, S. Shirai, T. Ohkame, T. Sakuma, M. Tanaka, N. Amano, A. Watanabe, H. Sakurai, T. Yamamoto, S. Yamanaka, A. Hotta, Precise correction of the dystrophin gene in Duchenne muscular dystrophy patient induced pluripotent stem cells by TALEN and CRISPR-Cas9. *Stem Cell Rev.* **4**, 143–154 (2015). doi:10.1016/j.stemcr.2014.10.013

15. D. G. Ousterout, A. M. Kabadi, P. I. Thakore, W. H. Majoros, T. E. Reddy, C. A. Gersbach, Multiplex CRISPR/Cas9-based genome editing for correction of dystrophin mutations that cause Duchenne muscular dystrophy. *Nat. Commun.* **6**, 6244 (2015). Medline doi:10.1038/ncomms7244

16. L. Xu, K. H. Park, L. Zhao, J. Xu, M. El Refaey, Y. Gao, H. Zhu, J. Ma, R. Han, CRISPR-mediated genome editing restores dystrophin expression and function in mdx mice. *Mol. Ther.* 10.1038/mt.2015.192 (2015).

17. J. C. van Deutekom, G. J. van Ommen, Advances in Duchenne muscular dystrophy gene therapy. *Nat. Rev. Genet.* **4**, 774–783 (2003). Medline doi:10.1038/nrg1180

18. E. Senís, C. Fatouros, S. Große, E. Wiedtke, D. Niopek, A. K. Mueller, K. Börner, D. Grimm, CRISPR/Cas9-mediated genome engineering: An adeno-associated viral (AAV) vector toolbox. *Biotechnol. J.* **9**, 1402–1412 (2014). Medline doi:10.1002/biot.201400046

19. F. Schmidt, D. Grimm, CRISPR genome engineering and viral gene delivery: A case of mutual attraction. *Biotechnol. J.* **10**, 258–272 (2015). Medline doi:10.1002/biot.201400529

20. H. Zhang, B. Yang, X. Mu, S. S. Ahmed, Q. Su, R. He, H. Wang, C. Mueller, M. Sena-Esteves, R. Brown, Z. Xu, G. Gao, Several rAAV vectors efficiently cross the blood-brain barrier and transduce neurons and astrocytes in the neonatal mouse central nervous system. *Mol. Ther.* **19**, 1440–1448 (2011). Medline doi:10.1038/mt.2011.98

21. C. N. Cearley, J. H. Wolfe, A single injection of an adeno-associated virus vector into nuclei with divergent connections results in widespread vector distribution in the brain and global correction of a neurogenetic disease. *J. Neurosci.* **27**, 9928–9940 (2007). Medline doi:10.1523/JNEUROSCI.2185-07.2007

22. D. Weber-Adrian, E. Thévenot, M. A. O'Reilly, W. Oakden, M. K. Akens, N. Ellens, K. Markham-Coultes, A. Burgess, J. Finkelstein, A. J. Yee, C. M. Whyne, K. D. Foust, B. K. Kaspar, G. J. Stanisz, R. Chopra, K. Hynynen, I. Aubert, Gene delivery to the spinal cord using MRI-guided focused ultrasound. *Gene Ther.* **22**, 568–577 (2015). Medline doi:10.1038/gt.2015.25

23. C. Bing, M. Ladouceur-Wodzak, C. R. Wanner, J. M. Shelton, J. A. Richardson, R. Chopra, Trans-cranial opening of the blood-brain barrier in targeted regions using a stereotaxic brain atlas and focused ultrasound energy. *J. Ther. Ultrasound* **2**, 13 (2014). Medline doi:10.1186/2050-5736-2-13

24. M. van Putten, E. M. van der Pijl, M. Hulsker, I. E. Verhaart, V. D. Nadarajah, L. van der Weerd, A. Aartsma-Rus, Low dystrophin levels in heart can delay heart failure in mdx mice. *J. Mol. Cell. Cardiol.* **69**, 17–23 (2014). Medline doi:10.1016/j.yjmcc.2014.01.009

25. C. Godfrey, S. Muses, G. McClorey, K. E. Wells, T. Coursindel, R. L. Terry, C. Betts, S. Hammond, L. O'Donovan, J. Hildyard, S. El Andaloussi, M. J. Gait, M. J. Wood, D. J. Wells, How much dystrophin is enough: The physiological consequences of different levels of dystrophin in the mdx mouse. *Hum. Mol. Genet.* **24**, 4225–4237 (2015). Medline doi:10.1093/hmg/ddv155

26. S. W. Cho, S. Kim, Y. Kim, J. Kweon, H. S. Kim, S. Bae, J. S. Kim, Analysis of off-target effects of CRISPR/Cas-derived RNA-guided endonucleases and nickases. *Genome Res.* **24**, 132–141 (2014). Medline doi:10.1101/gr.162339.113

27. S. Q. Tsai, Z. Zheng, N. T. Nguyen, M. Liebers, V. V. Topkar, V. Thapar, N. Wyvekens, C. Khayter, A. J. Iafrate, L. P. Le, M. J. Aryee, J. K. Joung, GUIDE-seq enables genome-wide profiling of off-target cleavage by CRISPR-Cas nucleases. *Nat. Biotechnol.* **33**, 187–197 (2015). Medline doi:10.1038/nbt.3117

28. X. Wang, Y. Wang, X. Wu, J. Wang, Y. Wang, Z. Qiu, T. Chang, H. Huang, R. J. Lin, J. K. Yee, Unbiased detection of off-target cleavage by CRISPR-Cas9 and TALENs using integrase-defective lentiviral vectors. *Nat. Biotechnol.* **33**, 175–178 (2015). Medline doi:10.1038/nbt.3127

29. K. J. Nowak, K. E. Davies, Duchenne muscular dystrophy and dystrophin: Pathogenesis and opportunities for treatment. *EMBO Rep.* **5**, 872–876 (2004). Medline doi:10.1038/sj.embor.7400221

30. F. A. Ran, P. D. Hsu, J. Wright, V. Agarwala, D. A. Scott, F. Zhang, Genome engineering using the CRISPR-Cas9 system. *Nat. Protoc.* **8**, 2281–2308 (2013). Medline doi:10.1038/nprot.2013.143

31. R. Willmann, A. De Luca, M. Benatar, M. Grounds, J. Dubach, J. M. Raymackers, K. Nagaraju, Enhancing translation: Guidelines for standard pre-clinical experiments in mdx mice. *Neuromuscul. Disord.* **22**, 43–49 (2012). Medline doi:10.1016/j.nmd.2011.04.012

32. V. Arechavala-Gomeza, M. Kinali, L. Feng, S. C. Brown, C. Sewry, J. E. Morgan, F. Muntoni, Immunohistological intensity measurements as a tool to assess sarcolemma-associated protein expression. *Neuropathol. Appl. Neurobiol.* **36**, 265–274 (2010). Medline doi:10.1111/j.1365-2990.2009.01056.x

33. K. Anthony, V. Arechavala-Gomeza, L. E. Taylor, A. Vulin, Y. Kaminoh, S. Torelli, L. Feng, N. Janghra, G. Bonne, M. Beuvin, R. Barresi, M. Henderson, S. Laval, A. Lourbakos, G. Campion, V. Straub, T. Voit, C. A. Sewry, J. E. Morgan, K. M. Flanigan, F. Muntoni, Dystrophin quantification: Biological and translational research implications. *Neurology* **83**, 2062–2069 (2014). Medline doi:10.1212/WNL.0000000000001025